

# Wind farm blockage effects: comparison of different engineering models

Emmanuel Branlard<sup>1</sup>, Eliot Quon<sup>1</sup>, Alexander R. Meyer Forsting<sup>2</sup>,  
Jennifer King<sup>1</sup>, Patrick Moriarty<sup>1</sup>

<sup>1</sup>National Renewable Energy Laboratory, Golden, CO, USA

<sup>2</sup>DTU Wind Energy, Technical University of Denmark Frederiksborgvej 399, 4000 Roskilde, Denmark

E-mail: [emmanuel.branlard@nrel.gov](mailto:emmanuel.branlard@nrel.gov)

**Abstract.** The work presents four engineering methods to estimate the induction zone in front of a wind turbine and account for the wind farm blockage effect. The methods comprise the vortex cylinder model, vortex dipole model, self-similar model, and wake projection model. The majority of the models presented account for yaw misalignments and ground effect. Actuator disk simulations are used to verify the individual models. The performance of each model is evaluated both in terms of precision and computational time. The induction models are coupled to wake models within the FLOW Redirection and Induction in Steady State framework to provide the full velocity field within a wind farm. Sample wind farm computations are presented, and the impact of including induction effects into wind farm performance predictions is reported. The different codes are publicly available online.

## 1. Introduction

The energy extraction from a wind turbine or wind farm induces a reduction of the upstream wind speed. This effect is referred to as “wind farm blockage,” and the affected area is called the induction zone.<sup>1</sup> Wind farm developers and owners have recently turned their attention to this area because current wind energy prediction procedures neglect wind farm blockage effects, resulting in an overprediction of farm production [1].

The first engineering model to account for induction effects in wind farms used a vortex-based model [2, 3]. Measurements of wind farm blockage using lidar technologies on full-scale wind farms can be found in research, such as in the work of Asimakopoulos [4]. Researchers have also studied the blockage effect using computational fluid dynamics (CFD) methods, primarily applying Reynolds-averaged Navier-Stokes (RANS) [5, 6, 1]. Currently, the computational expenses of the CFD simulations are too high to allow for layout optimizations. Accurate engineering models of the upstream and downstream flow of a turbine are thus essential for wind power plant design and performance optimization. Engineering wake models typically depend on the superposition of single-turbine wake models that may be based on first principles [7, 8]. However, the induction effects are generally not enforced in engineering and midfidelity

<sup>1</sup> In this work, the terms “induction zone” and “blockage effect” are used interchangeably. Large-scale array effects and the two-way interaction of the wind farm with the atmospheric boundary layer are not considered in this study.



**Table 1.** Features of the different models used in this study;  $\oplus$  and  $\otimes$  indicate increasing computational cost and efficiency, respectively.

Model	Radial Velocity	Near Rotor	Ground Effect	Yaw	Complexity
Actuator disk (AD)	✓	✓	✓	✓	$\oplus\oplus$
Wake projection (WP)	✓*	✓*	✓*	✓*	$\oplus$
Vortex cylinder (VC)	✓	✓	✓	✓	$\otimes$
Vortex dipole (VD)	✓	✗	✓	✓	$\otimes\otimes$
Self-similar (SS)	✗	✗	✓*	✗	$\otimes\otimes$

\* Added in the current study

tools. Induction effects are expected to gain importance for tightly packed and/or large turbine arrays.

This study intends to answer the following questions: How can the wind farm blockage effect be modeled using simple engineering models? How do the models perform compared to advanced numerical tools? How can engineering induction models be combined with wake models to provide the velocity field throughout a wind farm? How important is the induction effect for overall wind farm performance?

First, we present four engineering models of different levels of complexity: the vortex cylinder (VC) model [9, 3], the vortex dipole (VD) model [3], the self-similar (SS) model of Troldborg et al. [10], and the wake projection (WP) model, a novel approach applying a projection correction to a wake model. The engineering models are coupled with the FLOW Redirection and Induction in Steady State (FLORIS) framework [11, 12], and the specific requirements for this integration are discussed. Then, we verify the performance of each model against results from actuator disk (AD) RANS simulations for a single turbine and for a  $5 \times 5$  wind farm. Last, we provide an illustrative example for a large-scale wind farm. Discussions on the different models follow in light of their predictive performance and computational requirements.

## 2. Engineering models to compute the induction zone

### 2.1. Introduction

We use four engineering models in this study to evaluate the velocity field in the induction zone upstream of a turbine. We do not use the models to evaluate the wake velocity; this part of the flow field is left for engineering wake models to compute. We note that the WP model uses an engineering wake as a starting point; the resulting corrected velocity field corresponds, then, to the entire flow field. The engineering models do not intend to capture the interaction between the wind farm and the atmospheric boundary layer, and as such, no deep-array effects are captured by the models. Interactions with the shear profile are not considered. We present each induction zone model in subsequent sections and describe how they are combined with wake models to form a complete velocity field. The source code for each model is available online [13]. All models provide the induced velocity in the direction normal to the rotor plane, taken as the x-axis, positive downstream; four of the models provide lateral and vertical velocities as well. The adopted coordinate system is illustrated in Figure 1a. The radial coordinate,  $r$ , is used in place of the Cartesian coordinate,  $y$ , when the flow is assumed axisymmetric. A summary of the different features supported by the models is given in Table 1. In the table, the models are distinguished based on their capacity to: compute the radial velocity (or other Cartesian components), provide the velocity in the full domain,<sup>2</sup> account for the ground effect,

<sup>2</sup> The SS and VD models are only valid after a certain distance (typically  $-R$ ) upstream of the turbine, and thus are not valid near the rotor.

and account for yaw misalignment. Computational times are reported qualitatively in the table. Quantitative values are provided in Section 3.3.

## 2.2. Common features of the vortex and SS models

This section discusses the common features between the VC, SS, and VD models. The velocity field provided by the SS model can be thought to be induced by a vorticity distribution. From this consideration, the model can be integrated within FLORIS in the same way as the vortex models, and the ground effect can also be added to the SS model.

We express the vortex models and the SS model in terms of the tangential vorticity of the wake, noted  $\gamma_t$ , and expressed in m/s. We assume that the tangential vorticity is related to the axial induction factor on the rotor disk as:  $a = -\frac{\gamma_t}{2U_0}$ , where  $a$  is the induction factor,<sup>3</sup> and  $U_0$  is the axial free-stream velocity. Further, we assume that the vorticity is related to the rotor thrust coefficient,  $C_T$ , by the following relation:

$$\gamma_t = -U_0 \left[ 1 - \sqrt{1 - C_T} \right] \quad (1)$$

where  $U_0$  is the free-stream velocity.

For these three models, the ground effect is implemented by mirroring the vorticity distribution with respect to the ground. This approach enforces the “slip” (or “no-flow-through”) boundary condition at the ground (see Figure 1b).

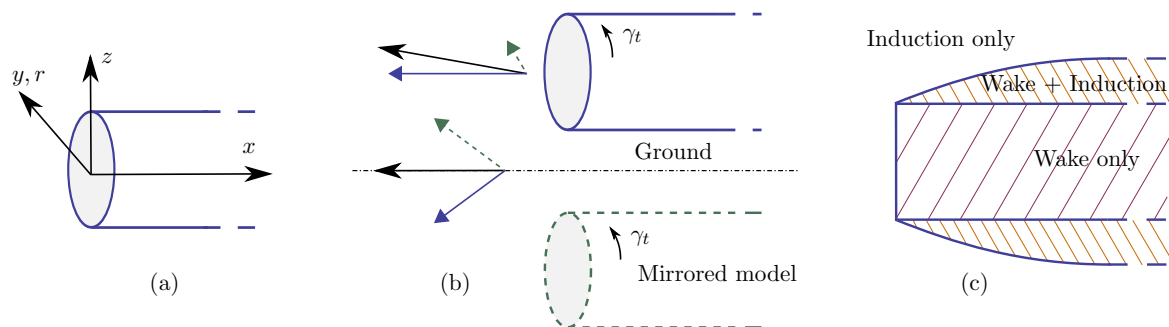


**Figure 1.** (a) Coordinate system. (b) Illustration of the mirroring technique for vorticity-based models. The sum of velocities induced by the vorticity above (blue) and below (green, dashed) the ground is such that the no-flow-through condition is respected at the ground. (c) Illustration of the superposition of induction models and wake models for a single turbine.

The three models are similarly implemented in FLORIS. The velocity from each model is used to account for induction effects but not for the wake effects. The different regions of the flow field are illustrated in Figure 1c. The velocity from the three induction models is set to 0 in the volume of the wake, chosen as the volume of a semi-infinite cylinder of radius,  $R$ , extending downstream from the rotor. Inside this volume, we use the velocity from the wake models of FLORIS. Outside this volume, we superpose the velocity field from the induction and wake models. This forms the baseline flow field about a turbine. When multiple turbines are present, we merge the wake velocities according to the methods implemented in FLORIS, whereas the induction velocities are superimposed to the background flow field. Because the induction effect affects the loading on the upstream turbine—whereas the wake affects the loading of the downstream turbine—we run iterations (usually 2) to ensure that the wind farm flow field and turbine loading are consistent. Further details are found in [3]. We continue by presenting each individual model.

<sup>3</sup> The motivation for choosing the vorticity as a main parameter, as opposed to the axial induction, is that the velocity at the rotor plane is often thought of as “induced” by the rotor loading and wake vorticity. This causality is yet arbitrary, and users can choose the axial induction as a main parameter.

### 2.3. The vortex cylinder (VC) model

The VC model prescribes the geometry of the wake to be a semi-infinite cylinder of constant intensity,  $\gamma_t$ . The velocity field is obtained by integrating the Biot-Savart law (e.g., [9, 3]). This model supports ground effect and yawed inflow. A single vortex cylinder is used in this study, but more advanced formulations can be used to account for the distribution of thrust along the rotor span and wake rotation effect.

### 2.4. The vortex dipole (VD) model

The VD model corresponds to a far-field approximation of the VC model. The induced velocity field is [3]:

$$u_x(r, x) = \frac{\gamma_t R^2}{4 r^2} \left[ \frac{x^3}{(x^2 + r^2)^{3/2}} - \frac{x}{(x^2 + r^2)^{1/2}} \right], \quad u_r(r, x) = -\frac{\gamma_t}{4} \frac{r R^2}{(x^2 + r^2)^{3/2}} \quad (2)$$

where  $R$  is the rotor radius. For a yawed configuration, we extend the model as follows:

$$u_x(\mathbf{x}) = \frac{\gamma_t R^2}{4} [x^2 I_{50} - 2x I_{51} + I_{52} - I_{30}], \quad u_y(\mathbf{x}) = \frac{\gamma_t R^2}{4} [xy I_{50} + m I_{52} - (mx + y) I_{51}] \quad (3)$$

$$u_z(\mathbf{x}) = \frac{\gamma_t R^2}{4} [xz I_{50} - z I_{51}]$$

with  $a^2 = x^2 + y^2 + z^2$ ,  $b = my + x$ ,  $c^2 = 1 + m^2$ , and

$$I_{30} = \frac{1}{a(ac - b)}, \quad I_{50} = \frac{2ac - b}{a^3(ac - b)^2}, \quad I_{51} = \frac{1}{a(ac - b)^2}, \quad I_{52} = \frac{1}{c(ac - b)^2}$$

where  $m = \tan \chi$  is the tangent of the wake skew angle. The formulae are singular on the doublet line: for points  $(x, mx, 0)$  with  $x > 0$ . Equations for this particular case are provided in [3]. The model includes ground effect via a mirroring of the vorticity with respect to the ground.

### 2.5. The self-similar (SS) model of Troldborg et al.

Troldborg et al. [10] derived an SS model of the axial-induced velocity, inspired by the solution of the SS plane jet:

$$u_x(r, x) = \frac{u_{x,a}(x)}{\cosh^\alpha \left( \frac{\beta r}{r_m(x)} \right)}, \quad u_{x,a}(x) = \frac{\gamma_t}{2} \left[ 1 + \frac{x}{\sqrt{x^2 + R^2}} \right], \quad r_m(x) = R \sqrt{\lambda \left( \eta + \frac{x^2}{R^2} \right)} \quad (4)$$

with  $\beta = \sqrt{2}$ ,  $\alpha = 8/9$ ,  $\lambda = 0.587$ , and  $\eta = 1.32$ . The model was calibrated using a set of RANS simulations obtained for different wind turbines and operating conditions. In Equation 4,  $u_{x,a}(x)$  corresponds to the velocity field induced by a vortex cylinder on the rotor axis. The SS model does not include the radial velocity and has not been derived for yawed inflows. The original model did not include the ground effect but is extended in the current work to account for this effect by using the mirroring technique discussed in Section 2.2.

### 2.6. The Wake Projection (WP) model

The projection approach estimates the entire velocity field, including the upstream induction field, by projecting the flow field provided by common wind turbine wake models, such as the Gaussian model [7, 14], into a divergence-free field. Because the wake model describes the mass flow through and momentum change imparted by an operational wind turbine, the problem is, therefore, to calculate a flow field that satisfies the conservation laws both upstream and

downstream. This is accomplished by enforcing continuity in the remainder of the flow field outside the modeled wake. Engineering wake models provide the wake velocity field,  $u_w$ , which is superposed to the free-stream velocity,  $U_0$ , to form the velocity field,  $\mathbf{u}_d$ :

$$\mathbf{u}_d(\mathbf{x}) = (U_0 + u_w(\mathbf{x})) \mathbf{e}_x, \quad (5)$$

where  $\mathbf{x}$  is an arbitrary point of the domain. The velocity field,  $\mathbf{u}_d$ , is nonsolenoidal at this point. We correct for the divergence of the velocity field by adding a correction,  $\mathbf{u}_c = \nabla\phi$ , where  $\phi$  is a velocity potential, determined by solving the following Poisson equation:

$$\nabla^2\phi(\mathbf{x}) = f(\mathbf{x}) = -\text{div } u_w. \quad (6)$$

Equation 6 is constrained by Neumann boundary conditions on all boundaries and is subject to the compatibility condition that  $\int f d\mathbf{x} = 0$ . Lastly, the projected velocity field within the domain is computed as:

$$\mathbf{u} = \mathbf{u}_d + \nabla\phi, \quad (7)$$

where  $\mathbf{u} = (u, v, w)$ . The boundary conditions imply that the velocity correction vanishes at the domain boundaries, therefore, automatically accounting for the ground effect because of  $w = -\frac{\partial\phi}{\partial z} = 0$  at the lower boundary, satisfying a no-flow-through condition. The ground effect can be neglected by solving Equation 6 on a domain with upper and lower boundaries equidistant and sufficiently far from the rotor.

Results for the projection model were calculated using the WP model within the FLORIS wake modeling framework [12]. Equation 6 was solved using second-order finite differences with the PyAMG library [15]. The solution domain extended 10 rotor radii from the edges of the rotor in all directions, with a point spacing of  $0.1R$  based on a preliminary grid convergence study in which 5, 10, and 20 points across the rotor disk were considered. A domain sizing study was also performed: for domain extents larger than  $10R$ , no appreciable change to the induction region—in which the local velocity was less than 95% of the freestream velocity—was observed.

### 3. Performance of the different models for a single turbine

#### 3.1. Reference simulations

AD RANS simulations were carried out using the Technical University of Denmark's 3D flow solver, EllipSys3D, developed by Michelsen and Sørensen [16, 17]. Results from these simulations are used as a reference to assess the quality of the velocity field obtained from the different models. The employed AD RANS setup has been validated previously with lidar velocity vector measurements of the induction zone in front of a full-scale wind turbine [18]. The maximal error in the averaged axial velocity remains below 1.3% beyond one rotor radius from the turbine. The RANS equations are closed by a  $k - \omega$  SST model, yet at the selected Reynolds number of 100 million, the flow field is essentially inviscid and the turbulence model is only active in the wake to stabilize the computations. Meyer Forsting et al. [19] showed that the turbulence model changes the velocities at most by 0.1% with respect to inviscid computations and that the signature of individual blades in the induction zone is lost with time averaging.

#### 3.2. Velocity field comparisons

A qualitative comparison of the velocity fields obtained using the different models for two  $C_T$  values is shown in Figure 2. Each plot shows contours of axial velocity as obtained from a given model and from the AD RANS simulation. As presented in previous studies, the VC model performs well in the entire induction zone compared to AD CFD. As expected, the VD model is not suitable for the flow near the rotor but captures the far-field flow with reasonable accuracy. Similar observations are made for the SS model, which was tuned by Troldborg et

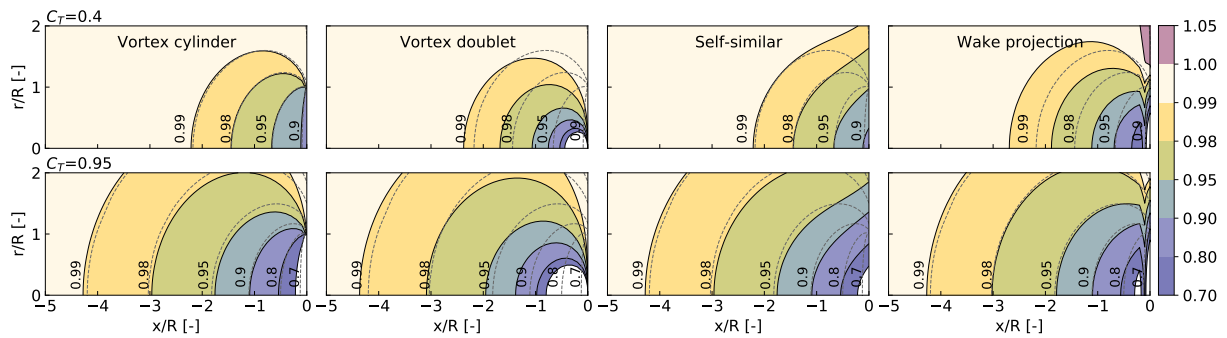


**Figure 2.** Comparison of the upstream axial velocity field  $((U_0 + u_x)/U_0)$  obtained using the different models (columns) for  $C_T = 0.4$  (top row) and  $C_T = 0.95$  (bottom row). The velocity contours from the AD RANS simulations are represented with dotted lines.

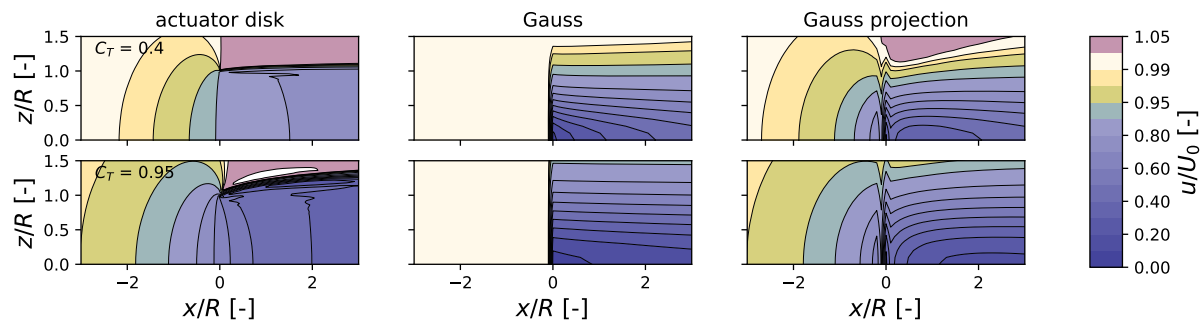


**Figure 3.** Comparison of the near-wake velocity fields predicted by the actuator disk and WP methods (left and right columns) for low- and high-thrust conditions (top and bottom rows, respectively). The middle Gauss column shows the initial velocity field predicted by the engineering wake model.

al. for flow further upstream than  $x = -R$ . The velocity field obtained with the WP model is in good agreement with the AD RANS simulations for the high  $C_T$  case, but the extent of the induction zone is overpredicted at low  $C_T$ . This can be attributed to a poor representation of the near wake by the engineering wake model at low  $C_T$ . As shown in Figure 3, the effect of the projection is to smoothly blend the far field and wake velocity fields in a manner that is physically consistent, thereby creating an appropriate upstream induction zone. Enforcing the divergence-free condition does not introduce additional body forces to the flow; therefore, it cannot significantly alter the initial wake velocity field. In comparison with the AD solution, the initial Gauss near wake for  $C_T = 0.4$  has a velocity deficit that is too large, contributing to increased blockage. For the  $C_T = 0.95$  case, even though the velocity deficit is slightly higher than predicted by the AD model, both the AD and WP provide the correct wake velocity in the far wake according to momentum theory; as a result, the WP model provides an excellent blockage prediction (shown in Figure 2). A closer look at the velocity profiles and a quantitative measure of the error are provided in the left and right of Figure 4, respectively. The relative error is computed in the area defined by  $(r/R, x/R) \in ([0, 0.9], [-5, -1])$ , where 20 points are used in the axial direction and 6 points in the radial direction.

Similar analyses are performed for a wind turbine located at  $1.5R$  above the ground, with ground effect included by the models. The results are presented in Figure 5. We observed that the overall ground-effect features of the axial velocity field are well-captured by the four models, with trends similar to the results without ground effect. Relative errors are provided in Figure 6.

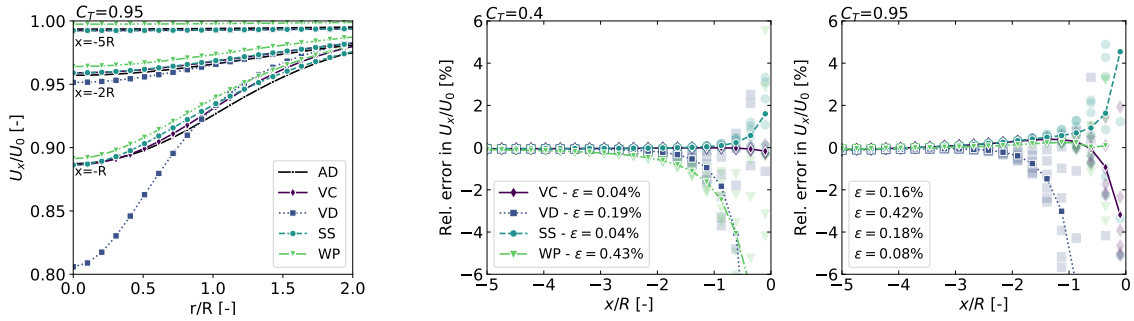


**Figure 4.** (Left:) Axial velocity field at the upstream positions,  $-R$ ,  $-2R$ , and  $-5R$ , for the different models at  $C_T = 0.95$ . (Middle and right:) Relative error in axial velocity of each model compared to the AD RANS simulations for  $C_T = 0.4$  (middle) and  $C_T = 0.95$  (right), as computed in the induction zone delimited by  $(r/R, x/R) \in ([0, 0.9], [-5, -1])$ . The error on a grid of  $20 \times 6$  points is shown with individual markers, whereas the mean is represented by a line. The mean of the absolute value of the relative error,  $\epsilon$ , is reported in the legend.

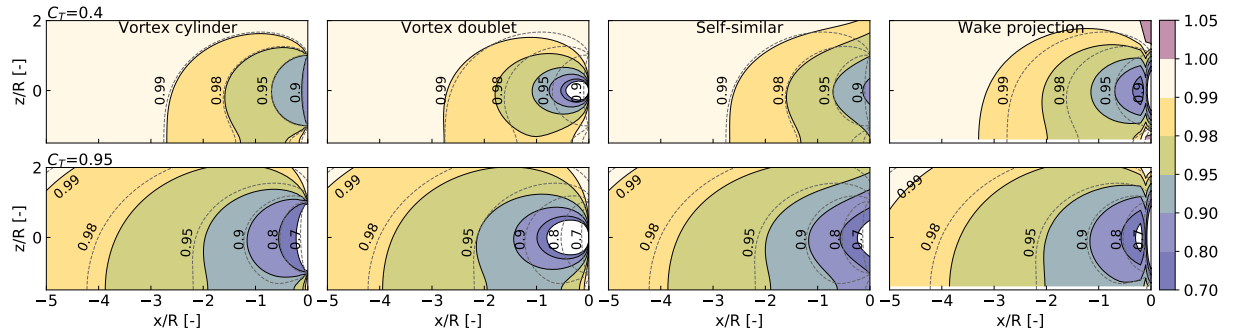


**Figure 5.** Ground effect. Comparison of axial velocity fields with AD results for the three models featuring the ground effect (VC, VD, and SS) for two thrust coefficients:  $C_T = 0.4$  (top row) and  $C_T = 0.95$  (bottom row). The ground is located at  $z = -1.5R$ .

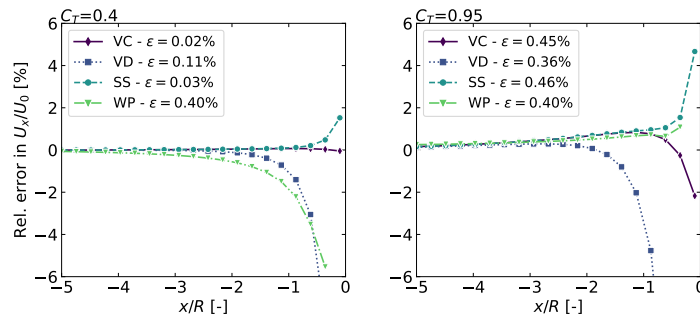


**Figure 6.** Relative error in the induction zone for the four different models, with ground effect included for  $C_T = 0.4$  (left) and  $C_T = 0.95$  (right). The induction zone is delimited by  $(z/R, x/R) \in ([-0.9, 0.9], [-5, -1])$ .

The relative errors are in the same order of magnitude as the ones obtained for the cases without ground effect shown in Figure 4.

### 3.3. Computational times

The AD and WP models are 3D models based on a velocity formulation, and thereby need to solve for the flow in the entire domain; their accuracy is a function of grid resolution. The other models are essentially grid-free and can compute the velocity at a single point without loss of accuracy. Typical computational times required by the different models to compute the velocity field around one wind turbine are reported in Table 2. For the contours shown in Figure 2,

**Table 2.** Typical computational times for the velocity field about one turbine. The AD and WP models require a large computational grid for accurate prediction. The VC, VD, and SS models are grid-free. The computational times for these models are provided for two grids: a grid of 5-M nodes to compare with the other methods, and the typical evaluation grid of 2,500 nodes used in this work.

Model	Language	Computational Grid	Time	Evaluation Grid	Time
AD	Fortran	$\approx 1M$	1.5 h		
WP	Python	$201 \times 221 \times 125 \approx 5M$	1.5 min		
VC	Python	$(170 \times 170 \times 170 \approx 5M)$	(2.5 min)	$50 \times 50$	0.01 s
VC+VD	Python	$(170 \times 170 \times 170 \approx 5M)$	(40 s)	$50 \times 50$	0.01 s
VD	Python	$(170 \times 170 \times 170 \approx 5M)$	(2.7 s)	$50 \times 50$	0.006 s
SS	Python	$(170 \times 170 \times 170 \approx 5M)$	(2.0 s)	$50 \times 50$	0.001 s

we only used 2,500 points, and results from the VC, VD, and SS models were obtained in a negligible time (less than 0.01 s). The AD and WP models used grids with orders of millions of cells. We ran the AD simulations on 8 processors for about 10 min. We run the WP model on a single CPU, with no parallelization techniques. Significant performance increases may be realized by rewriting the solver in C++ or FORTRAN. Furthermore, this approach would always be faster than a comparable turbulent RANS simulation since there is only a single solution step to perform the projection in steady state. Because the VD model corresponds effectively to the far-field velocity field of a vortex cylinder, the VC and VD models can be combined so that far-field velocities are computed with the VD model instead of the more expensive VC model. This is indicated with the line “VC+VD” in the table. Great speed-up can be obtained with this approach, in particular, for wind farm computations (this is the approach used in Section 4.2). In light of the results presented in the previous section, the VD model appears to provide a satisfying trade-off between accuracy and computational time. Yet, most of the engineering models presented provide velocity fields in times small enough to allow for rapid evaluation of the velocity field in the induction zone of one turbine.

#### 4. Evaluation of the different models for a wind farm

In this section, we present results for different wind farms: first, with an uncoupled model and second, with the fully coupled FLORIS integration. The uncoupled model is used to compare the models to AD RANS simulations. The WP model currently cannot be applied to wind farms of such scales because of the large number of grid cells necessary for such a problem. We discuss the necessary steps to apply the WP model to large problems in Section 3.3.

##### 4.1. Comparison of velocity fields for a $5 \times 5$ wind farm

We use a squared  $5 \times 5$  wind farm layout to compare the velocity fields from the different models in the induction zone of the wind farm. The wind turbine spacing is 5 diameters. The thrust coefficients of each turbine of the wind farm, obtained by the AD simulation, are used as input for all engineering models. This uncoupling is done to avoid differences in wakes between the models and the AD RANS simulation. We present fully coupled FLORIS simulations in Section 4.2. The velocity field in the induction zone of the wind farm, as obtained by the engineering models, is compared to the AD results in Figure 7. The velocity upstream of the middle row and top row are shown in the figure. We observe subtle differences in inductions between the two locations. The model errors tend to be smaller for the top row than the middle row, indicating that some second-order effects are missing from the simple superposition of velocity fields. Overall, we



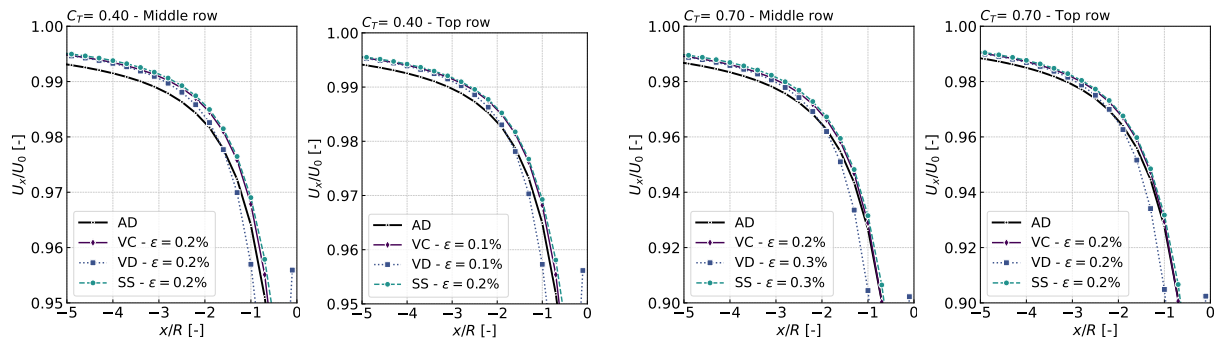


**Figure 7.** Axial velocity upstream of a  $5 \times 5$  wind farm for two  $C_T$  values ( $C_T = 0.4$  and  $C_T = 0.7$ ) and two rows: the middle row and top row.

observe an underestimation of the induction of around  $0.12U_0$  at  $x = -2.5D$  for all models. A calibration of the  $\gamma_t - C_T$  relationship can further reduce this error.

#### 4.2. Illustrative example using FLORIS

The four engineering models are integrated into FLORIS and combined with the wake calculation procedure, as described in Section 2. Regular FLORIS input files can be used to simulate a wind farm, and the different induction models are activated based on an additional input parameter. We close this work by showing an application of the model to the Anholt wind farm located in Denmark, comprising 111 turbines. We used the National Renewable Energy Laboratory's 5-MW reference rotor to avoid using data from the manufacturer. The results provided are thus not the ones that would be obtained for the real wind farm. The velocity field, as computed by FLORIS with the VC+VD model, is shown in Figure 8. For the condition simulated ( $U_0 = 8$  m/s), the induction effect reduced the average power produced by the wind farm by 0.33%. Examples of applications for the VC model for different wind sectors are found in [3]. Typical computational times for a grid of  $500 \times 500 \times 2$  for these layouts were about 1 min for the VC+VD model. The wake part of the FLORIS calculation took about 2 min. Computational times using the VD and SS models were of the order of 20 s. An AD RANS simulation for a wind farm of 63 turbines takes about 1 h using 170 cores.

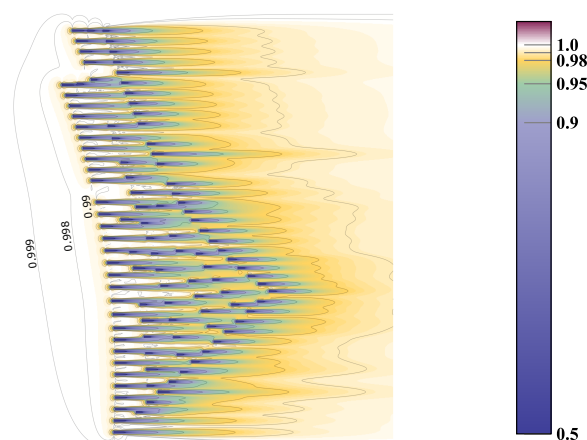


**Figure 8.** Velocity fields computed for the Anholt wind farm, using the combination of the Gaussian wake model from FLORIS and the VC+VD induction model.

## 5. Conclusions

Different models are now available in the open-source framework, FLORIS, to obtain the steady-state velocity field at every location in a wind farm, including the induction effect. The different models presented showed various levels of accuracy, with an average error level below 1% in the induction zone. The accuracy of the VC, VD, and SS models can be improved by tuning the relationship between  $C_T$  and  $\gamma_t$ . The accuracy of the WP model is strongly related to the accuracy of the modeled near wake. Making improvements to the FLORIS near-wake model is an active area of research.

For a single turbine, all engineering models have a definite computational time advantage compared to the AD simulations. The VC+VD, VD, and SS models require a negligible time for the velocity computation compared to the AD simulations. The WP model currently cannot be applied to large wind farms, but a number of additional numerical solutions and performance improvements can be achieved. We evaluated the right-hand side of the Poisson equation from discrete values; however, the gradients of the modeled wake velocity field may be obtained analytically. In addition, a more in-depth study into domain size and resolution requirements is underway. Finally, the solver can be further optimized to make use of advanced preconditioner and solver algorithms.

The models can easily be applied to different wind turbine layouts to assess blockage and wake effects and their impact on power production with different levels of fidelity. The effects of atmospheric stability are not captured by the models, whereas stability is known to have a strong impact on blockage effects. Future work should address this issue and also consider the performance of the models in a yawed condition.

## Acknowledgements

This work was authored by the National Renewable Energy Laboratory, operated by Alliance for Sustainable Energy, LLC, for the U.S. Department of Energy (DOE) under Contract No. DE-AC36-08GO28308. Funding provided by the U.S. Department of Energy Office of Energy Efficiency and Renewable Energy Wind Energy Technologies Office. The views expressed in the article do not necessarily represent the views of the DOE or the U.S. Government. The U.S. Government retains and the publisher, by accepting the article for publication, acknowledges that the U.S. Government retains a nonexclusive, paid-up, irrevocable, worldwide license to publish or reproduce the published form of this work, or allow others to do so, for U.S. Government purposes.

## References

- [1] Blegg, J., Purcell, M., Ruisi, R. & Traiger, E. Wind farm blockage and the consequences of neglecting its impact on energy production. *Energies* **11**, 1609 (2018).
- [2] Branlard, E. & Meyer Forsting, A. Using a cylindrical vortex model to assess the induction zone in front of aligned and yawed rotors. In *Proceedings of EWEA Offshore 2015 Conference* (2015).
- [3] Branlard, E. & Meyer Forsting, A. R. Assessing the blockage effect of wind turbines and wind farms using an analytical vortex model. *Wind Energy* **23**, 1–20 (2020).
- [4] Asimakopoulos, M., Clive, P. & Boddington, R. Offshore compression zone measurement and visualization. In *Proceedings of the European Wind Energy Association 2014 Annual Event (Barcelona, Spain)* (2014).
- [5] Nishino, T. & Draper, S. Local blockage effect for wind turbines. *J. Phys. Conf. Ser.* **625** (2015).
- [6] Meyer Forsting, A. R., Troldborg, N. & Gaunaa, M. The flow upstream of a row of aligned wind turbine rotors and its effect on power production. *Wind Energy* **20**, 63–77 (2017).
- [7] Bastankhah, M. & Porté-Agel, F. A new analytical model for wind-turbine wakes. *Renew. Energ.* **70**, 116–123 (2014).
- [8] Martinez-Tossas, L. A., Annoni, J., Fleming, P. A. & Chruuchfield, M. J. The aerodynamics of the curled wake: a simplified model in view of flow control. *Wind Energ. Sci.* **4**, 127–138 (2019).
- [9] Branlard, E. & Gaunaa, M. Cylindrical vortex wake model: right cylinder. *Wind Energy* **18**, 1–15 (2014).
- [10] Troldborg, N. & Meyer Forsting, A. R. A simple model of the wind turbine induction zone derived from numerical simulations. *Wind Energy* **20**, 2011–2020 (2017).

- [11] Annoni, J. *et al.* Analysis of control oriented wake modeling tools using lidar field results. *Wind Energy science* **3**, 819–831 (2018).
- [12] NREL. FLORIS. Version 1.0.0. <https://github.com/NREL/floris> (2019).
- [13] Branlard, E. WIZ, wake and induction zone model <https://github.com/ebranlard/wiz> (2019).
- [14] Abkar, M. & Porté-Agel, F. Influence of atmospheric stability on wind-turbine wakes: A large-eddy simulation study. *Physics of Fluids* **27**, 035104 (2015).
- [15] Olson, L. N. & Schroder, J. B. PyAMG: Algebraic multigrid solvers in Python v4.0. <https://github.com/pyamg/pyamg> (2018).
- [16] Michelsen, J. A. *Block Structured Multigrid Solution of 2D and 3D elliptic PDE's*. (AFM 94-05 - Department of Fluid Mechanics, Technical University of Denmark, 1994).
- [17] Sørensen, N. N. *General Purpose Flow Solver Applied to Flow over Hills*. Ph.D. thesis, Risø National Laboratory. (1995).
- [18] Meyer Forsting, A. *et al.* Validation of a CFD model with a synchronized triple-lidar system in the wind turbine induction zone. *Wind Energy* **20**, 1481–1498 (2017).
- [19] Meyer Forsting, A. R., Troldborg, N., Bechmann, A. & Réthoré, P.-E. *Modelling Wind Turbine Inflow: The Induction Zone*. Ph.D. thesis, DTU Wind Energy, Denmark (2017).